

Diffusion-Limited Binary Reactions: The Hierarchy of Nonclassical Regimes for Correlated Initial Conditions

Katja Lindenberg*

Department of Chemistry and Institute for Nonlinear Science, University of California at San Diego, La Jolla, California 92093-0340

Panos Argyrakis† and Raoul Kopelman

Departments of Chemistry and Physics, The University of Michigan, Ann Arbor, Michigan 48109-1055

Received: October 15, 1993; In Final Form: December 22, 1993*

We predict hierarchies of kinetic regimes and crossover conditions for elementary $A + A \rightarrow 0$ and $A + B \rightarrow 0$ batch reactions from a nonclassical reaction–diffusion formalism that includes spatial fluctuations. This paper addresses the case of a spatially correlated initial distribution of reactants; random initial conditions have been discussed in another paper. The hierarchies of kinetic regimes are even richer than those found for random initial conditions, with the particular hierarchy determined by the tightness of the initial correlations. In most cases there is one regime (which we call a “burst”) where the decay of the densities in the $A + B$ reaction is even *faster* than in the $A + A$ reaction. We confirm our predictions via detailed numerical simulations.

1. Introduction

The spontaneous formation of nonuniform spatial structures associated with diffusion-limited binary reactions in low dimensions has been widely studied in the past few years. These nonuniform spatial distributions manifest themselves through “anomalous” rate laws for the global densities $\rho(t)$ of the reacting species.^{1–27} For example, the irreversible reaction $A + A \rightarrow 0$ under “normal” circumstances is described by the rate law $\dot{\rho} = -k\rho^2$ whereas the asymptotic rate law for dimensions $d < 2$ in an infinite volume is $\dot{\rho} = -k\rho^{(1+2/d)}$.^{1,4,21–27} The slowdown implied by the larger exponent is a consequence of the deviation of the spatial distribution of A's from the Hertz distribution of nearest-neighbor distances.²⁸ The Hertz distribution has a maximum at zero separation and leads to the normal rate law. The nearest-neighbor distribution underlying the anomalous rate law has many fewer close reactant pairs.^{1,15,27} This nonrandom distribution arises from the fact that diffusion is not an effective mixing mechanism in low dimensions.²⁹

The diffusion-limited irreversible reaction $A + B \rightarrow 0$ also exhibits anomalous kinetics in low dimensions. Under normal circumstances the rate laws for the global densities ρ_A and ρ_B are $\dot{\rho}_A = \dot{\rho}_B = -k\rho_A\rho_B$. If $\rho_A(t=0) = \rho_B(t=0) \equiv \rho(t=0)$, then the densities of the two species are equal at all times and we can dispense with the subscripts so that once again $\dot{\rho} = -k\rho^2$. The actual asymptotic rate law in an infinite volume in dimensions $d < 4$ for an initially random distribution of reactants is instead $\dot{\rho} = -k\rho^{(1+4/d)}$. In this system the principal cause of the anomalous behavior is the formation of aggregates of like particles.^{1–20} The spatial regions in which the density of one type of particle is overwhelmingly greater than that of the other grow in time (while the total density within each aggregate of course decreases with time). Since the reaction can essentially only occur at the interfaces between aggregates, and since the number of these interfaces decreases with time, the reaction slows down relative to the rate that would describe a random mixture of reactants. Again, this behavior reflects the fact that diffusion is not an effective mixing mechanism in low dimensions. Initial spatial fluctuations in relative densities can thus grow in size as the reaction that eliminates close opposite pairs proceeds.

This evolution of the $A + B \rightarrow 0$ reaction is predicated on the presence of initial spatial fluctuations in the reactant densities. Indeed, the specific rate law $\dot{\rho} = -k\rho^{(1+4/d)}$ depends on an initial distribution of reactants that is completely random. The situation changes with a different initial particle distribution, although anomalies will in any case be associated with initial fluctuations. Such fluctuations, even if different from those associated with a completely random distribution, will tend to grow (at least initially) but may lead to an asymptotic exponent different from $(1 + (4/d))$, and the critical dimension for anomalous behavior may in general differ from $d = 4$.

In this paper we outline the various regimes of kinetic behavior of the densities of reactants for the reaction $A + B \rightarrow 0$ from the initial time until the asymptotic behavior is reached when initially correlated A–B pairs are randomly placed in the system.³⁰ The corresponding analysis for a random initial distribution of reactants has been presented elsewhere.³¹ We characterize the various kinetic regimes and estimate the crossover times from one regime to another. Initial pair correlations clearly limit the initial (and hence subsequent) fluctuations in the particle numbers and hence they affect the rate laws. We present numerical simulation results in one dimension and analyze these results in terms of our model. Our analysis also offers insight into the behavior of the $A + A \rightarrow 0$ reaction. Most of the details omitted from this presentation are included in a review presented elsewhere.³³

Much of our analysis is based on the reaction–diffusion model for the local densities $\rho_A(\mathbf{r}, t)$ and $\rho_B(\mathbf{r}, t)$:^{6,31,32}

$$\dot{\rho}_A(\mathbf{r}, t) = D\nabla^2\rho_A(\mathbf{r}, t) - k_1\rho_A(\mathbf{r}, t)\rho_B(\mathbf{r}, t) \quad (1)$$

and similarly for $\rho_B(\mathbf{r}, t)$, where k_1 is the time-independent local rate coefficient and D is the diffusion coefficient for both species. It turns out to be convenient to deal instead with the difference and sum variables^{6,31,32} $\gamma(\mathbf{r}, t) \equiv 1/2[\rho_A(\mathbf{r}, t) - \rho_B(\mathbf{r}, t)]$ and $\rho(\mathbf{r}, t) \equiv 1/2[\rho_A(\mathbf{r}, t) + \rho_B(\mathbf{r}, t)]$. The difference variable satisfies the linear diffusion equation $\dot{\gamma}(\mathbf{r}, t) = D\nabla^2\gamma(\mathbf{r}, t)$ which can of course be solved exactly. The sum variable satisfies the equation obtained by summing (1) and its partner for ρ_B :

$$\dot{\rho}(\mathbf{r}, t) = D\nabla^2\rho(\mathbf{r}, t) - k_1[\rho^2(\mathbf{r}, t) - \gamma^2(\mathbf{r}, t)] \quad (2)$$

This equation is more difficult to deal with and can only be handled approximately.

* Permanent address: Department of Physics, University of Thessaloniki, GR-54006 Thessaloniki, Greece.

† Abstract published in *Advance ACS Abstracts*, March 1, 1994.

In section 2 we specify in detail the initial conditions to be considered in this paper and consider the behavior of the difference variable for these initial conditions. Section 3 describes our simulation methods. Section 4 summarizes our results for random initial conditions.³¹ Section 5 deals with the sum variable equation for the correlated initial distribution of reactants, the kinetic regimes that might be observed as the densities decay from their initial distributions, and the crossover times from one kinetic behavior to another. We also present simulation results and analyze them in terms of our theoretical predictions. Section 6 presents our conclusions and a brief overall summary of our results.

2. Initial Conditions and Difference Equation

We deal with the situation in which N molecules of type A and N molecules of type B are initially placed in the system at locations $\{\mathbf{r}_j^A\}$ and $\{\mathbf{r}_j^B\}$ with $j = 1, \dots, N$, respectively. Here we consider the case of A–B pairs that are deposited at random locations, but in such a way that the members of each pair are constrained to be a distance c apart.³⁰ Different A–B pairs may interpenetrate. The initial distribution can then be written as a product of pair distributions $p(\mathbf{r}_j^A, \mathbf{r}_j^B)$, $j = 1, \dots, N$, where the probability density for each A–B pair is

$$p(\mathbf{r}^A, \mathbf{r}^B) = \frac{\Gamma(d/2)}{2V\pi^{d/2}} \int d\Omega \delta(\mathbf{r}^B - \mathbf{r}^A - \mathbf{c}) \quad (3)$$

Here \mathbf{c} is a vector of length c and random orientation and the integration is over these orientations, and $\Gamma(x)$ is the gamma function.

The difference variable satisfies the linear diffusion equation, which can be solved exactly.^{31,33} The quantity of interest involving the difference variable is its mean square value $\langle \gamma^2(\mathbf{r}, t) \rangle$ (see below), where the brackets indicate an average over the initial distribution of reactants. One easily finds³³

$$\langle \gamma^2(\mathbf{r}, t) \rangle = Q t^{-d/2} (1 - e^{-c^2/8Dt}) \rightarrow Q \frac{c^2}{8D} t^{-(d+2)/2} \quad (4)$$

where the last expression is valid for times $t \gg c^2/8D$ and where $Q \equiv \rho_0/2(8\pi D)^{d/2}$.

Our Monte Carlo simulations are performed on discrete lattices. The lattice sites are separated by lattice constant a , and the total number of lattice sites is L , so that $V = La^d$. In the continuum limit $a \rightarrow 0$ and $L \rightarrow \infty$ such that V remains finite. The continuum densities $\rho(\mathbf{r}, t)$ and $\gamma(\mathbf{r}, t)$ have units of number per unit volume, while in our simulations we deal with densities in units of number per lattice site. Denoting the lattice densities by $\rho^{\text{lat}}(l, t)$ where the index l labels the lattice sites, we have the relation $\rho \sim \rho^{\text{lat}}/a^d$. The maximum value of ρ^{lat} when multiple occupancy of a site is not allowed is thus unity. In order to simplify notation in our discussion of simulation results in subsequent sections, we will in general omit the superscript "lat" even when dealing with lattice densities since the usage will be clear from the context.

The diffusion coefficient D in the discretized problem has the value $D = 1/2$ (the distance scale implicit in the diffusion coefficient is thus different in different dimensions). The correlation distance is discretized by writing $c = \lambda a$, where λ is the number of lattice constants that separates a correlated pair.

3. Method of Simulations

The simulations are performed using the conventional techniques described in our earlier papers.^{15,34,35} In this paper we restrict our simulations to one dimension. Briefly, lattices of sizes up to 10^6 sites are generated. We do not allow multiple occupancy of sites. The A–B correlated pairs are placed on the lattice so that the A particle and B particle of each pair are placed exactly λ sites apart. This is accomplished by first positioning the A particle on a random site on the lattice provided it is

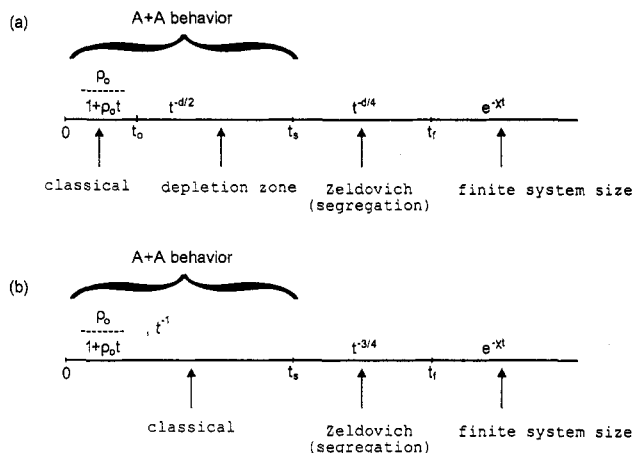


Figure 1. Possible time progressions of kinetic behaviors for a random initial condition: (a) $d \leq 2$; (b) $d = 3$.

unoccupied. Then its B partner is placed in one of the two possible sites which is exactly λ sites away from the A. The choice is again made at random. If the chosen site happens to be occupied by another particle, then the other choice is tested. If both sites at a distance λ sites away are occupied, then the pair is totally removed from the system and a new effort is initiated to position the pair somewhere else on the lattice. Cyclic boundary conditions are used, so that it is possible for an A–B pair to be split at the ends of the lattice. The reaction process proceeds in the usual way: The particles diffuse on the lattice by performing independent random walks to nearest-neighbor sites (thus carrying no further memory of their counterpart). Two A's or two B's are not allowed to occupy the same site. If an A and a B step onto the same site they react, which means that they are removed from the system. Cyclic boundary conditions are employed for the random walk as well. We monitor the particle density as a function of time for times ranging up to 10^8 steps.

4. Kinetic Behavior for Random Initial Conditions

The kinetic behaviors that arise in the $A + B \rightarrow 0$ reaction with correlated initial conditions are particularly interesting when compared to the behavior of the same reaction with random initial conditions. Here we summarize the results obtained elsewhere^{31,33} for the average density $\langle \rho(\mathbf{r}, t) \rangle$ of either species for the case of random initial conditions.

In our earlier work,³¹ we introduced the following terminology: By *classical* behavior we mean the decay appropriate to the classical rate law $\dot{\rho} = -k\rho^2$, that is, $\langle \rho(\mathbf{r}, t) \rangle = \rho_0/(1 + k\rho_0 t)$. The terminology *depletion zone* behavior denotes the nonclassical behavior exhibited, for example, in an $A + A \rightarrow 0$ or an $A + A \rightarrow A$ reaction because of the "depletion zone" that forms around each surviving reactant after the initially very close pairs have quickly reacted. It is characterized by the decay law $\langle \rho(\mathbf{r}, t) \rangle \sim t^{-d/2}$ for $d \leq 2$ and $\langle \rho(\mathbf{r}, t) \rangle \sim t^{-1}$ for $d > 2$,^{15,19,21} with logarithmic corrections when $d = 2$.^{15,34-37} In the *Zeldovich* or *segregation* regime the segregation of species dominates the kinetic behavior embodied in the well-known $\langle \rho(\mathbf{r}, t) \rangle \sim t^{-d/4}$ behavior for $d \leq 4$ (again with possible logarithmic corrections when $d = 4$) and classical behavior for $d > 4$.^{1-5,15,16} Finally, in the *finite system size* regime the decay of the average density is exponential in time.

A possible kinetic progression for random initial conditions is shown in Figure 1 for one dimension. At early times the $A + B \rightarrow 0$ reaction behaves the same as the $A + A \rightarrow 0$ reaction. Both exhibit classical behavior at very early times but quickly cross over to the depletion zone behavior. We do not provide an estimate for the crossover time t_0 but simulations indicate that it is extremely short (on the order of a few stepping times). The depletion zone behavior continues until the average density is of order $\rho_s \sim f_d \rho_0$,

where f_d is a dimension-dependent fraction. Our simulations lead to the values $f_d \sim 0.3$ – 0.5 in one dimension, and $f_d \sim 0.03$ in two dimensions. The time t_s at which the average density has the value ρ_s is of order

$$t_s \sim \frac{1}{8\pi\rho_0^{2/d}f_d^{4/d}} \quad (5)$$

After the time t_s , segregation effects begin in the A + B reaction and the Zeldovich regime sets in. This behavior continues until a time t_f at which finite system size effects are felt. Finite size effects begin when the average linear size of each kind of aggregate (which grows in time as $t^{1/2}$) is within an order of magnitude of the size of the system. In one dimension our simulations lead to $t_f/L^2 \sim 2 \times 10^{-3}$ for all values of L simulated. In two dimensions we find $t_f/L^2 \sim 4 \times 10^{-2}$. In this progression we have assumed that finite size effects set in long after the onset of the Zeldovich regime, that is, $t_f \gg t_s$. This need of course not be the case: as the system size decreases t_f sets in earlier and earlier.

5. Kinetic Behavior for Correlated Initial Conditions

Our analysis is based primarily on the ensemble average of (2) over the initial distribution of reactants:

$$\langle \dot{\rho}(\mathbf{r}, t) \rangle = D\nabla^2 \langle \rho(\mathbf{r}, t) \rangle - k_1 [\langle \rho^2(\mathbf{r}, t) \rangle - \langle \gamma^2(\mathbf{r}, t) \rangle] \quad (6)$$

Note that the squared difference variable $\langle \gamma^2(\mathbf{r}, t) \rangle$ appears as a source term in the reaction–diffusion equation: the fluctuations in the difference variable thus drive the dynamics of the system. For random initial conditions $\langle \gamma^2(\mathbf{r}, t) \rangle = Q t^{-d/2}$. Comparison with (4) confirms that random initial conditions allow for greater fluctuations in the difference variable than do correlated initial conditions. This difference lies at the root of the differences in the dynamical behavior of the systems with different initial conditions.

The continuum limit places constraints on parameter values and variables—if these constraints are not met, a continuum approach makes no sense. One of these constraints is that the correlation distance c must be sufficiently large for there to be many particles between each correlated pair; i.e., we must have $\langle \rho(\mathbf{r}, t) \rangle c^d \gg 1$. This condition can at best hold only up to some time t —once $\langle \rho(\mathbf{r}, t) \rangle$ becomes sufficiently small the condition is necessarily violated. Nevertheless, we can still argue heuristically about some features of the behavior of the system even at very low densities.

To proceed from this point one must find a way to deal with the quantity $\langle \rho^2(\mathbf{r}, t) \rangle$ and, in particular, with its relation to $\langle \rho(\mathbf{r}, t) \rangle$. Rather than attempting to construct a hierarchy of ever higher powers involving ρ and γ , we proceed along the following lines.

First, we calculate $\langle \rho^2(\mathbf{r}, 0) \rangle$ exactly. Assuming that at most one molecule can be placed at each lattice site we obtain^{31,33}

$$\langle \rho^2(\mathbf{r}, 0) \rangle = \langle \rho(\mathbf{r}, 0) \rangle^2 + \rho_{\max} \langle \rho(\mathbf{r}, 0) \rangle = \rho_0^2 + \rho_{\max} \rho_0 \quad (7)$$

Here we have dropped terms of $O(N/V^2)$. The quantity $\rho_{\max} \equiv 1/2a^d$ is the highest possible density of each reactant in the simulations with which our results will subsequently be compared. In a continuum model $a \rightarrow 0$ and $\rho_{\max} \rightarrow \infty$. However, we retain ρ_{\max} as a finite quantity to represent the effect of the finite size of the A and B molecules and the resultant excluded volume effect. Note that the first term on the right-hand side of (7) is at most equal to the second.

Our analysis of the random initial condition case³¹ was based on the appearance of a number of length scales whose interplay determines the way in which the system evolves: the distance between nearest neighboring particles, the linear size of an aggregate of like particles, and the size of the system. In the

current analysis a fourth length scale occurs, namely, the distance c initially separating a correlated A–B pair. This additional length leads to a rich variety of new behavior determined by its size relative to that of the other scales.

The entire crux of non-classical reaction kinetics is the departure of $\langle \rho^2(\mathbf{r}, t) \rangle$ from the relation (7). To characterize this departure we write³¹

$$\langle \rho^2(\mathbf{r}, t) \rangle = \eta \langle \rho(\mathbf{r}, t) \rangle^2 + \mu \rho_{\max} \langle \rho(\mathbf{r}, t) \rangle \quad (8)$$

which constitutes a definition of η and μ . We argue below that the variation of μ between 1 and 0 (and, less importantly, that of η between 1 and $1/2$) captures all the important kinetic regimes of the A + B \rightarrow 0 reaction.

5.1. Kinetic Regimes. We begin our analysis by assuming that the continuum condition holds at least initially, that is, $\rho_0 c^d \gg 1$, and will later comment of the behavior of the system when this is not the case.

The first kinetic regime occurs at $t = 0$. The analysis of this regime parallels that of the random initial condition³¹ since at very early times reacting pairs of particles are not correlated pairs—the latter are still too far apart. Instead, reactions involve uncorrelated partners coming from different correlated pairs and the dynamics is therefore indistinguishable from the random initial condition. Thus, as in the random case we first note in eq 6 that the diffusion term vanishes at $t = 0$ since $\langle \rho(\mathbf{r}, 0) \rangle = \rho_0$ is independent of \mathbf{r} . The average $\langle \rho^2(\mathbf{r}, 0) \rangle$ is given in (7). Clearly, (4) is inappropriate for the evaluation of the initial mean square difference variable [the difficulty arises from the limits that have been taken in evaluating (4)]. Direct evaluation gives instead^{31,33}

$$\langle \gamma^2(\mathbf{r}, 0) \rangle = \rho_{\max} \langle \rho(\mathbf{r}, 0) \rangle = \rho_{\max} \rho_0 \quad (9)$$

[the infinity in (4) as $t \rightarrow 0$ arises from the fact that in the strict continuum limit $\rho_{\max} \rightarrow \infty$]. Thus, eqs 7 and 9 in (6) at $t = 0$ yield

$$\langle \dot{\rho}(\mathbf{r}, t) \rangle|_{t=0} = -k_1 \langle \rho(\mathbf{r}, 0) \rangle^2 \quad (10)$$

the *classical rate equation* for a bimolecular reaction. Thus, very near $t = 0$ we have $\langle \rho(\mathbf{r}, t) \rangle = \rho_0 / (1 + k_1 \rho_0 t)$.

Note that at $t = 0$ the average of the product $\langle \rho_A \rho_B \rangle$ separates exactly into the product of the averages, $\langle \rho_A(\mathbf{r}, 0) \rho_B(\mathbf{r}, 0) \rangle = \langle \rho_A(\mathbf{r}, 0) \rangle \langle \rho_B(\mathbf{r}, 0) \rangle$. The analysis that leads to classical behavior at very early times is unstable to any fluctuations that lead to a deviation from this strict equality. These fluctuations are of course embodied in $\langle \gamma^2(\mathbf{r}, t) \rangle$. Thus, as soon as these fluctuations destroy the equality so that $\langle \rho_A(\mathbf{r}, t) \rho_B(\mathbf{r}, t) \rangle \neq \langle \rho_A(\mathbf{r}, t) \rangle \langle \rho_B(\mathbf{r}, t) \rangle$, another kinetic behavior determined by the associated nonrandom distribution necessarily sets in. Contiguous pairs of A and B molecules will react quickly, and unless diffusion can just as quickly replenish such pairs, there will be deviations from a random distribution as reflected in the inequality.

Since (4) is an exact result, deviations from the initial random distribution of correlated pairs are already built into it. In (8) deviations from randomness appear in the deviation of μ and η from unity. However, as long as μ is still of $O(1)$, the second term on the right-hand side of (8) dominates the first.

In order to balance contributions of various terms in (6) so as to establish the time dependence of $\langle \rho(\mathbf{r}, t) \rangle$ in the time regime where the distribution of reactants may no longer be strictly random but μ is still of $O(1)$, we explicitly substitute (4) and (8) into (6):

$$\langle \dot{\rho}(\mathbf{r}, t) \rangle = D\nabla^2 \langle \rho(\mathbf{r}, t) \rangle - k_1 [\eta \langle \rho(\mathbf{r}, t) \rangle^2 + \mu \rho_{\max} \langle \rho(\mathbf{r}, t) \rangle - Q t^{-d/2} (1 - e^{-c^2/8Dt})] \quad (11)$$

The dominant balances depend not only on η and μ but also on the relative importance of the exponential contribution to the last

term. This contribution is the sole consequence of the correlated initial conditions. The exponential becomes important at times $t \sim t_c$, where t_c is proportional to the time that it takes on the average for a particle to cover a distance c ,

$$t_c \equiv c^2/8D \quad (12)$$

At times greater than t_c correlated particles have had an opportunity to meet one another; at times prior to t_c correlated particles "do not know" of one another's existence and the system should therefore behave as with a random initial condition. This is indeed the case; the differences between the random and correlated systems only set in beyond time t_c , and the entire further analysis depends on where this time falls in relation to the other characteristic times of the system. This is another way of saying that the subsequent behavior depends on the relation of the length scale c to the other characteristic length scales introduced earlier.

If t_c is much greater than the (extremely short) time t_0 , then the transition from classical to A + A depletion zone behavior will again occur at time t_0 (as in the random initial condition problem). Beyond this time, the dominant time dependence of $\langle \rho(\mathbf{r}, t) \rangle$ for $d = 1$ must be of the form

$$\langle \rho(\mathbf{r}, t) \rangle \sim \frac{Q}{\mu \rho_{\max}} t^{-1/2} \quad (13)$$

The largest terms in (11) then balance each other. For $d \geq 2$ the dominant balance is established with the leading behavior (with perhaps logarithmic corrections in time in two dimensions) $\langle \rho(\mathbf{r}, t) \rangle \sim t^{-1}$. When $d = 2$ the dominant balance involves the diffusion term, the term linear in the density, and the Q term in (11). In dimensions $d \geq 3$ the Q term becomes unimportant.

In this "intermediate" time regime we thus find that the main time dependence of the mean density goes as $\langle \rho(\mathbf{r}, t) \rangle \sim t^{-d/2}$ for $d \leq 2$ and as t^{-1} for $d > 2$, exactly as in the case of random initial conditions. This behavior is nonclassical in one dimension and is completely analogous to the nonclassical regime of the A + A \rightarrow 0 and A + A \rightarrow A reactions.^{15,19,21}

The subsequent behavior of the system depends on the relative magnitudes of the time t_s introduced in (5) and the time t_c . Recall that the time t_s marks the beginning of the aggregation process in the random initial condition case and the consequent slowing down of the reaction. If t_s is smaller than t_c then the evolution of the correlated system continues as that of the random system and segregation begins to set in before the correlation length is felt by associated partners. If, on the other hand, $t_s \gg t_c$ then the correlation effects are felt before segregation sets in, segregation does not occur, and the behavior is quite different. We discuss these two cases separately.

5.1.1. Dynamics with Segregation. Consider first the case $t_s \ll t_c$. With the explicit expressions (5) and (12) this condition can be translated to the statement

$$c^d \rho_0 \gg \frac{1}{\pi^{d/2} f_d^2} \quad (14)$$

In one dimension our simulation results led to $f_d \sim 0.3 - 0.5$,³¹ so that (14) requires that $c \rho_0 \gg 6$: if this condition is satisfied, then segregation sets in at time t_s as in the random initial condition case. In two dimensions we found $f_d \sim 0.03$ ³¹ so that segregation sets in at time t_s provided that $c^2 \rho_0 \gg 350$. Note that with condition (14) both in one and two dimensions the density of the system at time t_s still satisfies the condition for the continuum approximation to be applicable, that is, $c^d \rho_s \sim c^d f_d \rho_0 \gg 1$. This is as it should be, since true segregation implies the existence of many particles separating correlated partners.

Our analysis captures the behavior of the system in the segregation regime if we set $\mu = O(\langle \rho \rangle / \rho_{\max})$ and $\eta = 1/2$ in (8). The choice $\eta = 1/2$ implies a complete segregation of species, i.e.,

that $\langle \rho_A(\mathbf{r}, t) \rho_B(\mathbf{r}, t) \rangle = 0$. This choice is not crucial to the term balancing arguments. More important is the choice of μ . One might be tempted to assume that the $t^{-d/4}$ behavior is mainly due to the macroscopic segregation and that the spatial distribution of molecules within each aggregate is of lesser importance. This is not the case: indeed, were we to assume an essentially random distribution within each aggregate we would set $\mu \approx 1$ and we would be back to the previous analysis, with the result that $\langle \rho(\mathbf{r}, t) \rangle \sim t^{-d/2}$ for $d \leq 2$. In reality the formation of macroscopic aggregates is accompanied by a nonrandom (clumped up) distribution within each aggregate.^{15,16} Hence the choice $\mu \ll 1$. We will see that setting $\mu = O(\langle \rho \rangle / \rho_{\max})$ captures the proper behavior. Thus in this regime in place of eq 11 we now analyze the balances implicit in

$$\langle \dot{\rho}(\mathbf{r}, t) \rangle = D \nabla^2 \langle \rho(\mathbf{r}, t) \rangle - k_1 [\alpha \langle \rho(\mathbf{r}, t) \rangle^2 - Q t^{-d/2}] \quad (15)$$

where $\alpha = O(1)$.

For $d \leq 4$ the dominant balance must occur inside the square brackets, whence

$$\langle \rho(\mathbf{r}, t) \rangle \sim (Q/\alpha)^{1/2} t^{-d/4} \quad (16)$$

For $d > 4$ a balance occurs if $\langle \rho(\mathbf{r}, t) \rangle \sim t^{-1}$ (classical behavior).

Segregation continues until time t_c is reached: at this time the exponential contribution to the last term in (11) becomes important and the balance of terms changes. Note that the average density ρ_c at this time is still sufficiently high for the continuum approximation to be valid (as expected): an estimate of ρ_c can be obtained from the relation $\rho_c \sim (t_c/t_s)^{-d/4} \rho_s$ which leads to the expression $c^d \rho_c \sim (c^d \rho_0)^{1/2} / \pi^{d/4}$. With $c^d \rho_0 \gg 1$ we then satisfy the continuum condition for $c^d \rho_c$ as well.

At and beyond times $t \sim t_c$ the exponent in eq 11 can be expanded and (11) can be rewritten as

$$\langle \dot{\rho}(\mathbf{r}, t) \rangle = D \nabla^2 \langle \rho(\mathbf{r}, t) \rangle - k_1 \left[\eta \langle \rho(\mathbf{r}, t) \rangle^2 + \mu \rho_{\max} \langle \rho(\mathbf{r}, t) \rangle - \frac{Q c^2}{8D} t^{-(d+2)/2} \right] \quad (17)$$

At time t_c the system is still segregated; since in general the size of an aggregate at time t is of the order of the region covered by a random walker in time t (at least in dimensions $d \leq 2$, where random walks are compact), the average linear dimension of the aggregates of like particles at time t_c is $\sim c$, the correlation distance of initially correlated pairs. The coefficient η in (17) is of $O(1)$ while $\mu \sim O(0)$, and the dominant balance then immediately leads to

$$\langle \rho(\mathbf{r}, t) \rangle \sim t^{-(d+2)/4} \quad \text{for } d \leq 2 \\ \sim t^{-1} \quad \text{for } d > 2 \quad (18)$$

The decay of the density in (18) is not only faster than that of the segregation regime but, for $d \leq 2$, indeed even faster than in the A + A depletion zone regime! This behavior comes about because the correlated initial condition places a limit of order c on the size of a segregated aggregate—the segregation pattern cannot continue beyond that. The initial correlations suppress fluctuations in relative densities of A and B particles that would be necessary for the growth of the segregation pattern to continue. Indeed, as time increases beyond t_c and the overall density of particles continues to decrease due to the reaction, so does the number of like particles in an aggregate relative to the total number of particles. As a consequence, the relative number of A–B interfaces at which the reaction can take place thus increases. This "shrinkage" of aggregates leads to the rapid decay in (18).³⁰

Eventually a configuration is reached where each A particle is essentially surrounded by B's and vice versa; the aggregates have now "shrunk" to single particles. This occurs at a time that

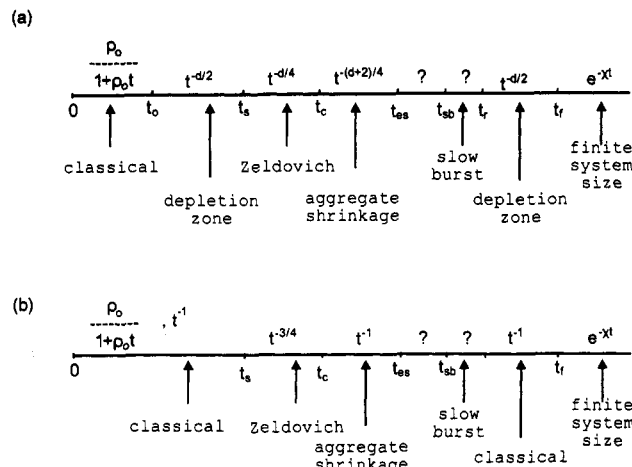


Figure 2. Possible time progressions of kinetic behaviors for a correlated initial condition when the initial particle density is sufficiently high for there to be a segregation regime: (a) $d \leq 2$; (b) $d = 3$.

we call t_{es} (the subscript stands for "end of shrinkage") at an average density ρ_{es} determined from the fact that the only surviving particles in the aggregates of size c are those in the center of the aggregates, that is, such that

$$c^d \rho_{es} \sim O(1) \quad (19)$$

These surviving particles are at a distance of order c apart. It is important to note that in general A–B pairs that are now a distance c apart are *not* originally correlated partners since chances are that the correlation partner of any given particle has already reacted. Thus, although the configuration at this point is reflective of and due to the original correlations, it reflects these original correlations in a somewhat indirect way. The time t_{es} can be estimated from the relation $\rho_{es} \sim (t_c/t_{es})^{-(d+2)/2} \rho_0$, which leads to

$$\left(\frac{t_{es}}{t_c}\right) \sim \left(\frac{c^d \rho_0}{\pi^{d/2}}\right)^{1/(d+2)} \quad (20)$$

Note that the times t_{es} and t_c become ever closer with decreasing c and decreasing ρ_0 . Therefore, to clearly see the aggregate shrinkage regime we should deal with large values of c (for given ρ_0). This in turn requires that the simulation be carried out to very long times.

At time t_{es} the condition (19) indicates that the continuum approximation has ceased to be valid, so that further arguments must be heuristic. A–B pairs are now narrowly distributed around a distance c , so after a time that is narrowly distributed around $\sim c^2/2D$ they will meet and react. Until this happens, the density does not change much. Thus at a time of order

$$t_{sb} \sim t_{es} + c^2/2D \sim t_{es} + t_c \quad (21)$$

we expect a sharp increase in the reaction rate. We call this a "slow burst" (hence the subscript sb; see below for further discussion of bursts and slow bursts). Following the slow burst, the system returns to the uncorrelated depletion zone A + A behavior ($t^{-d/2}$) at a time t_r , a behavior that may be overshadowed by the onset at t_f of finite system size effects. Finite size effects lead to exponential decay of the density when $\langle \rho \rangle \sim 1/L^d$, that is, when the average distance between particles is of the order of the size of the system.

Figure 2 summarizes the progression of kinetic behaviors discussed above.

5.1.2. Dynamics without Segregation. Next consider the situation where the correlation distance is sufficiently short that correlation effects set in before segregation can occur, that is, t_c

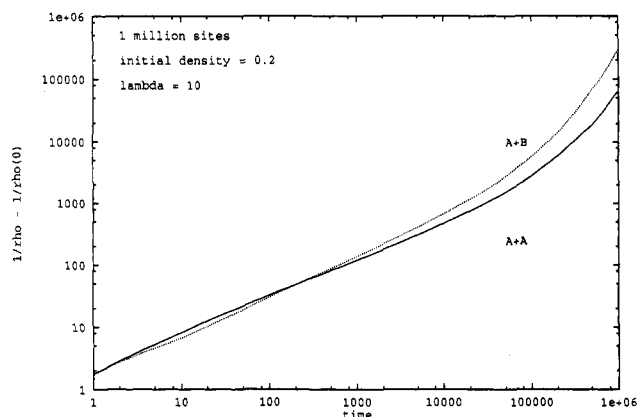


Figure 3. $\langle \rho \rangle^{-1} - \rho_0^{-1}$ vs t in one dimension with a fairly tightly correlated initial condition for the initial density $\rho_0 = 0.2$. The evolution for the two reactions is very similar.

$< t_s$. In this case even if $c^d \rho_0 > 1$ initially, $c^d \langle \rho(r,t) \rangle$ becomes of $O(1)$ at time t_c while the system is still in the A + A depletion regime or perhaps even in the classical behavior mode. Our arguments in this regime are therefore necessarily heuristic since the continuum approximation is no longer valid. Note that in this case there should be no distinction between the A + B and A + A problems over the entire time regime; that is, initially tightly correlated A + A's should evolve in exactly the same way as initially tightly correlated A + B's. Indeed, Figure 3 is a typical simulation in this regime that shows the reactant density for both reactions. In this particular one-dimensional simulation $c \rho_0 = 2$. As we will see below, when the initial pairs are even more tightly correlated, the two reactions evolve even more equally.

It is easier to discuss first the very low initial density case, $c^d \rho_0 < 1$. An important behavior-determining feature then is the fact that with the exception of a few uncorrelated pairs that were initially closer than distance c and that may therefore react before time t_c , originally correlated pairs are now able to react because they have an opportunity to encounter one another before either partner has reacted with another molecule. This fact, coupled with the fact that correlated pairs started out at exactly a distance c apart, means that at times very narrowly distributed around t_c many pairs suddenly encounter one another and the reaction rate suddenly experiences a sharp (short-lived) burst. We thus expect the density to experience a sharp decrease at times $t \sim t_c$. Note that this burst due to the reaction of correlated partners is not observed in the high-initial-density case, but that a remnant of this effect is observed (the "slow burst"). Once the burst is over because most of the initially correlated pairs have reacted with one another (time t_r), the situation reverts back to that of the uncorrelated A + A problem since each remaining particle is essentially surrounded by uncorrelated particles of the opposite kind. The system thus never reaches the Zeldovich regime, and the asymptotic behavior for an infinite system is $t^{-d/2}$ ($d \leq 2$) and t^{-1} ($d \geq 3$). The return to the depletion zone behavior may again be overshadowed by finite size effects.

Next consider the case $c^d \rho_0 > 1$ (but $c^d \rho_0$ not sufficiently large for segregation to occur). In this case there is still a burst that sets in at around t_c , albeit a slow one (reflective of the initial interpenetration of correlated pairs). This slow burst is consistently observed for both A + A \rightarrow and A + B \rightarrow reactions.

Figure 4 summarizes the progression of kinetic behaviors discussed above.

5.2. Comparison with Monte Carlo Simulations. Figure 5 shows the Monte Carlo simulation results for one-dimensional lattices of one million sites with cyclic boundary conditions for various correlated initial conditions. The initial density in all cases is 0.2 particles of each species per lattice site. The discrete correlation distance λ is indicated on each curve. The "random" curve corresponds to the random initial condition.

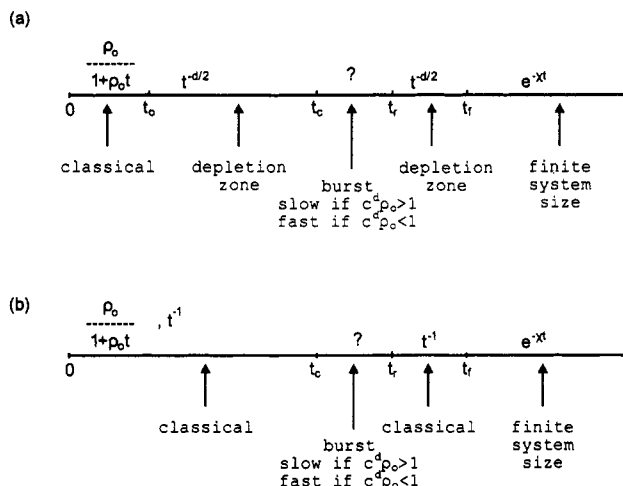


Figure 4. Possible progressions of kinetic behaviors for a correlated initial condition when the initial particle density is not sufficiently high for there to be a segregation regime: (a) $d \leq 2$; (b) $d = 3$.

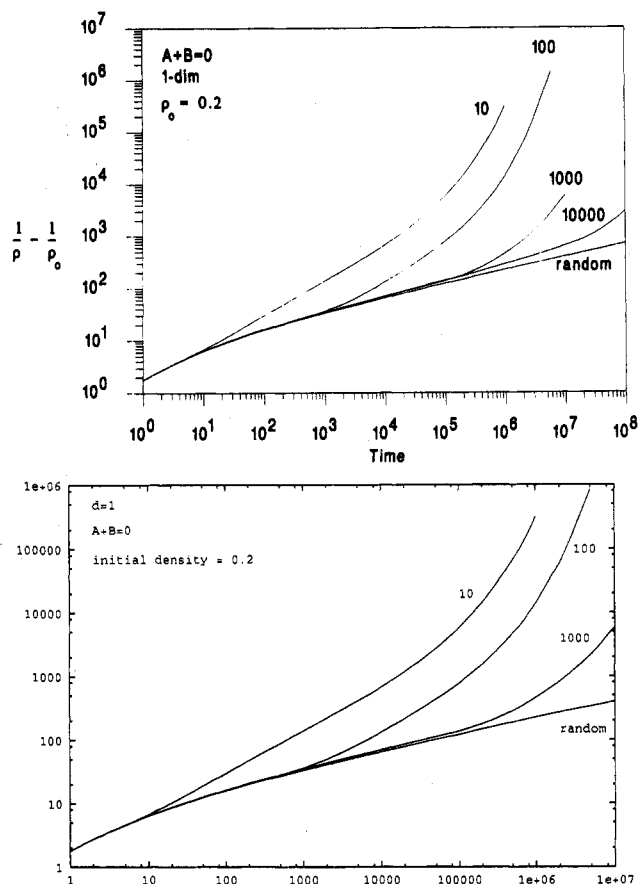


Figure 5. $(\rho)^{-1} - \rho_0^{-1}$ vs t for one-dimensional lattices of one million sites with various correlation lengths λ as indicated in the figures. The initial density of each species in all cases is $\rho_0 = 0.2$. Parts a and b differ in the time length of the simulations. The "random" curves in both are for a random initial condition.

The behavior of the "random" curve was discussed in detail in ref 31. In particular, we pointed out that the initial slope of this curve overlaps that of a direct $A + A$ simulation; that is, it is initially classical (slope 1) but very quickly crosses over to the $t^{-1/2}$ behavior characteristic of the depletion zone regime. We find that the "average slope" over the first 10 steps is 0.55. At very long times the Zeldovich behavior becomes apparent: the last decade of the simulation leads to an average slope of 0.249. The crossover time from the depletion zone behavior to the Zeldovich behavior is found to be $t_2 \sim 10^2$. Finite lattice size effects are not yet apparent over the time scales shown.

Now consider the $\lambda = 10\,000$ curve in Figure 5a, for which $\rho_0\lambda = 2000 \gg 6$. The expected kinetic progression for this case is as shown in Figure 2a. The time t_s should occur in the same region as for the random initial condition since t_s is independent of the correlation distance. Earlier we found that, for $\rho_0 = 0.2$, $t_s \sim 10^2$. The independence of t_s from λ is indeed observed in Figure 5a—the two curves are superimposed for times that are much longer than t_s . The faster decay of the $\lambda = 10\,000$ density is expected to set in at about $t_c = \lambda^2/8D = 2.5 \times 10^7$, consistent with the behavior observed in the figure. Indeed, we find that in the range 2×10^7 to 10^8 the average slope of the curve is 0.77, that is, close to the predicted $3/4$. The reactant density predicted from eq 20 at t_c is $\rho_c \sim 3 \times 10^{-3}$, which is consistent with the density obtained from Figure 5a at t_c . The crossover time into the slow burst regime, t_{sb} , is predicted to occur at about 10^8 , that is, an order of magnitude greater than t_c . This is beyond our time scale. However, we do see the beginning of a sharp increase in the reaction rate, perhaps indicative of the expected slow burst.

Next consider the $\lambda = 1000$ curve in Figure 5b. Now $\rho_0\lambda = 200 \gg 6$, so the expected kinetic progression is again as shown in Figure 2a. The time $t_s \sim 10^2$ is still well within the regime where the $\lambda = 1000$ curve is essentially the same as the random initial condition curve. The faster decay of the density when $\lambda = 1000$ is expected to set in at $t_c = \lambda^2/8D = 2.5 \times 10^5$, which is consistent with the behavior observed in the figure. The reactant density predicted at this onset is $\rho_c \sim 10^{-2}$, which is again consistent with the density obtained from the figure at t_c . The crossover into the slow burst regime is predicted to occur at $t_{sb} \sim 10^6$, only a factor of 5 above t_c . This range is too narrow to extract a reliable slope in this range, even though the curve does go through a slope of $3/4$ within the range. A sharp increase beyond the slope of $3/4$ is clearly observed in the last decade of the simulation, indicative of the slow burst.

For the $\lambda = 100$ case, with $\rho_0\lambda = 20$, we are still in the kinetic progression of Figure 2a, but some of the kinetic regimes become extremely narrow. The curve hugs the random curve beyond time $t_s \sim 10^2$ and into the Zeldovich regime, but the time $t_c = 2.5 \times 10^3$ is only about an order of magnitude beyond t_s . Therefore the slope $1/4$ is never achieved; instead, the lowest observed slope is $1/3$. The time t_{sb} in turn is only about twice t_c . Therefore, the slow burst starts almost immediately beyond t_c . Each simulation for $\lambda = 100$ is ended when only about one particle of each type remains.

When $\lambda = 10$ we have the situation with the kinetic progression shown in Figure 4a (with a slow burst). This is the same curve as the $A + B$ curve in Figure 3. Here the progression goes directly from the $t^{-1/2}$ behavior to the slow burst regime. Again, simulations were ended when only about one particle of each type remains.

Note that a return from the slow burst to an uncorrelated $A + A$ behavior is not observed in any of the cases shown in Figure 5b. Presumably finite system size effects obfuscate this regime.

In Figure 6 we consider a number of one-dimensional cases that fall within the parameter regimes of "dynamics without segregation", that is, appropriate to the kinetic regimes shown in Figure 4a, both with $\lambda\rho_0 < 1$ and with $\lambda\rho_0 > 1$. The solid curves are the $A + B$ simulations. As a baseline for comparison we include the curve for a random initial distribution of reactants. This is the same as the $\rho_0 = 0.002$ curve in Figure 4 of ref 31. We see that almost the entire random curve lies in the $A + A$ depletion zone regime ($t^{-1/2}$), and only in the last time decade in Figure 6 is there a beginning of the crossover into the Zeldovich regime. The time t_s is about 10^6 . The dashed line in the figure is the result of $A + A \rightarrow 0$ simulations with $\rho_0 = 0.002$ and random initial condition. The $A + A$ and $A + B$ curves are clearly similar until the crossover of the $A + B$ curve begins. The long-time slope of the dashed line is 0.56.

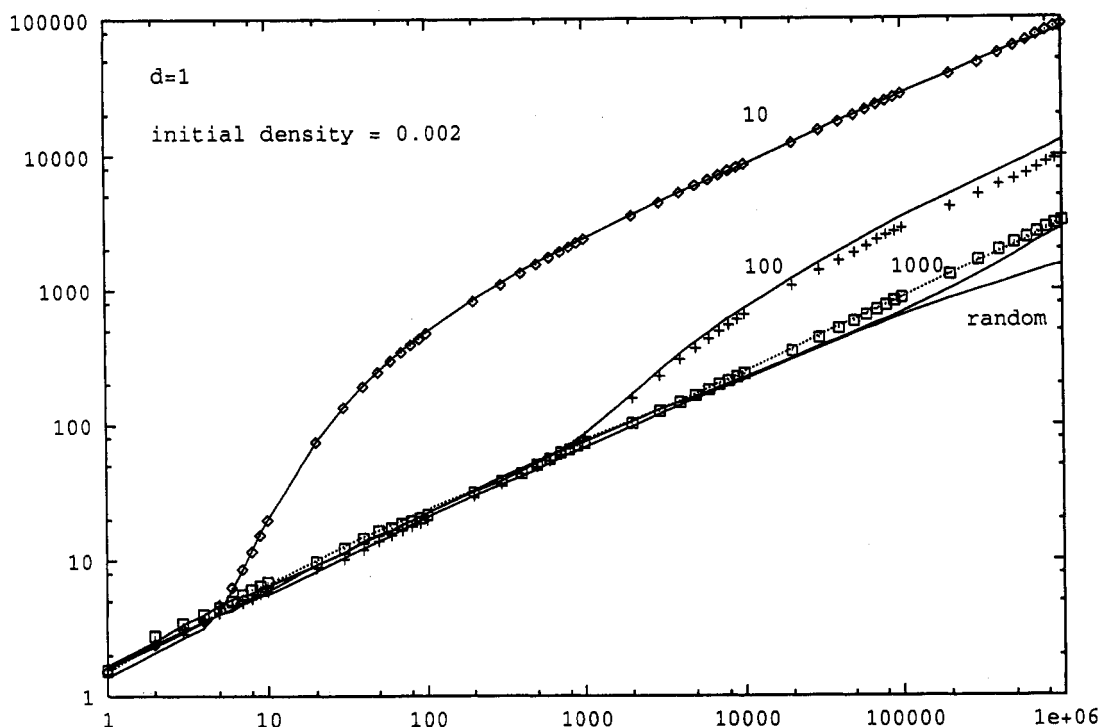


Figure 6. $\langle \rho \rangle^{-1} - \rho_0^{-1}$ vs t for one-dimensional lattices of one million sites with various correlation lengths λ as indicated. The initial density of each species in all cases is $\rho_0 = 0.002$. The solid curves are for the $A + B \rightarrow 0$ simulations. The dashed curve is for simulations of the reaction $A + A \rightarrow 0$ with random initial conditions. The symbols are for $A + A$ simulations with $\lambda = 10$ (diamonds), $\lambda = 100$ (pluses), and $\lambda = 1000$ (squares).

Let us now discuss the finite λ cases, starting with the smallest value of λ . The solid curve is the $A + B$ simulation and the diamonds are the results of $A + A \rightarrow 0$ simulations. As stated in our earlier discussion in the context of dynamics without segregation, we expect (and indeed see) essentially identical behavior of the two in this tightly correlated situation. Since $\rho_0\lambda = 0.02 \ll 1$, we expect to be squarely within the "fast burst" kinetic progression of Figure 4a. Indeed, at early times the $\lambda = 10$ curve hugs the random initial condition curve. The time $t_c = 25$ is within the range of the observed fairly sharp burst. Once the burst is over, the curve reverts to the expected $t^{-1/2}$ behavior: the observed slope is 0.52. Finite system size effects are not reached within this simulation.

When $\lambda = 100$ we are still in the "fast burst" regime of Figure 4a since $\rho_0\lambda = 0.2 < 1$. The solid curve for the $A + B$ simulation and the +'s for the $A + A$ simulation are almost the same (the initial correlations are of course not as tight as for $\lambda = 10$). The curve again hugs the random initial condition curve, and the burst crossover time is expected at about $t_c = 2500$. This is again well within the crossover region. Beyond the burst the slope again reverts to the expected $1/2$ (the actual value is 0.53).

When $\lambda = 1000$ we have $\rho_0\lambda = 2$, that is, we now expect a slow burst rather than a fast burst. Note that $\rho_0\lambda$ has the same value as for the curves in Figure 3. The solid curve is the $A + B$ curve, the squares are the simulations for $A + A$ with $\lambda = 1000$, and recall that the dashed curve is for $A + A \rightarrow 0$ with random initial conditions. The three curves are obviously very close. The slow burst is expected to begin at $\sim 2.5 \times 10^5$, and the $A + B$ curve may show an early indication of this effect.

Next we consider Figure 7, where we show the curves for the $A + B$ reaction in one dimension with $\lambda = 10$ for various initial densities. The $\rho_0 = 0.002$ curve is the same as the $\lambda = 10$ curve in Figure 6, and the $\rho_0 = 0.2$ curve is the same as the $\lambda = 10$ curve in Figure 5b. Figure 7 illustrates the transition from the kinetic progression involving a fast burst to one involving a slow burst in Figure 4a. The most notable observation is the fact that the density curves cross; that is, at long times a system with an initially higher density has fewer particles left than one with an initial density 10 or even 100 times lower! These crossings must be a

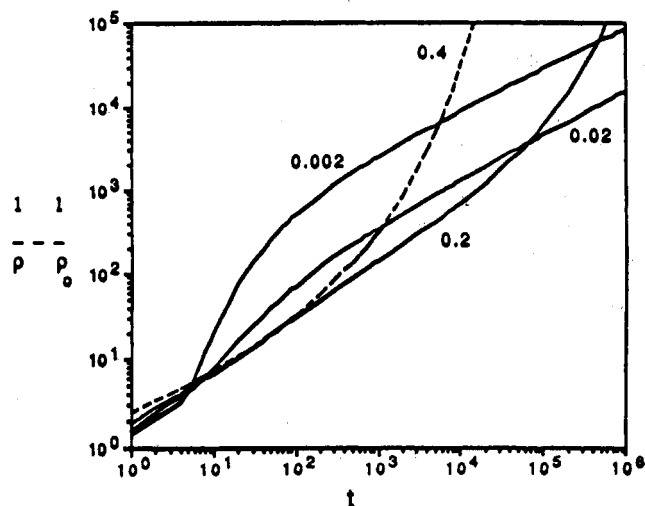


Figure 7. $\langle \rho \rangle^{-1} - \rho_0^{-1}$ vs t for different initial densities. In all cases $A-B$ pairs are initially placed $\lambda = 10$ sites apart.

consequence of the different particle distributions in the different cases, leading to a rate that is not just dependent on the value of the global density. For the $\rho_0 = 0.02$ and the $\rho_0 = 0.002$ curves the long time slopes are $1/2$ and the interparticle distributions are those characteristic of the $A + A$ depletion zone, that is, a skewed exponential.^{1,15,27} For the $\rho_0 = 0.2$ curve we do not know the particle distribution, but it clearly must be different.

Figure 8 is similar to Figure 7 but now $\lambda = 100$. The crossover t_c is expected at 2.5×10^3 . The $\rho_0 = 0.02$ curve ($\rho_0\lambda = 0.2 < 1$) shows a fast burst in that regime, and the 0.2 and 0.4 curves ($\rho_0\lambda = 20$ and 40) exhibit slow bursts starting about then (note that the 0.2 curve is the same as the $\lambda = 100$ curve in Figure 5b). The $\rho_0 = 0.02$ curve (which, with $\rho_0\lambda = 2$, is in the slow burst regime) marks the transition between the fast burst and slow burst behavior. Note that both the 0.02 and 0.002 curves have slopes of about $1/2$ before as well as after the burst. Thus, this figure clearly illustrates the change in behavior from the slow burst that follows the aggregate shrinkage (Figure 2a) through

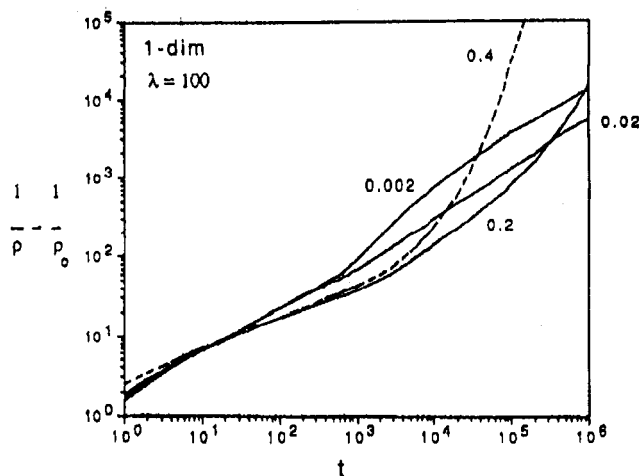


Figure 8. $\langle \rho \rangle^{-1} - \rho_0^{-1}$ vs t for different initial densities. In all cases A-B pairs are initially placed $\lambda = 100$ sites apart.

the slow burst in the absence of segregation to the fast burst (Figure 4a) as $\rho_0\lambda^d$ decreases. For fixed λ we expect the onset of these various bursts to occur at about the same time, $t \sim t_c = \lambda^2/8D$, as indeed they do in Figure 8 at around $t \sim 2.5 \times 10^3$.

6. Discussion

In this section we summarize the highlights of our findings, following the kinetic progressions shown in Figures 2 and 4.

In all cases, as in the random case,³¹ at early times the A + B reaction behaves in the same way as the A + A reaction. At some point deviations from this behavior begin, and the different progressions differ in the time and nature of these deviations. The differences are mainly determined by the relative magnitudes of the characteristic times t_s and $t_c = \lambda^2/8D$. If $t_s < t_c$ then as in the random case segregation begins around time t_s , while if $t_c < t_s$ there is no segregation regime. In the latter case the A + B \rightarrow 0 reaction behaves in the same way as the A + A \rightarrow 0 reaction for a given ρ_0 and λ throughout the entire kinetic progression. Thus our work has not only elucidated the behavior of the A + B reaction with correlated initial conditions but also that of the A + A reaction with correlated initial conditions, which to the best of our knowledge has not previously been done.

Let us begin with the case $t_s > t_c$, that is, when there is no segregation. In particular, we begin with the most tightly correlated initial conditions (Figure 4), $c^d\rho_0 < 1$. At time t_c there is a sudden increase in the reaction rate, a "fast burst", because the initially correlated pairs meet with a high probability. This burst is fairly sharp (decreasingly so with increasing $\rho_0\lambda^d$) and, once it is over, the "normal" A + A behavior $t^{-d/2}$ sets in again. This behavior continues until finite size effects set in at very low densities. This analysis is borne out quantitatively by our simulations.

Consider next the less tightly correlated case where $\rho_0\lambda^d > 1$ but not sufficiently large for segregation to occur. In one dimension $1 < \rho_0\lambda < 6$ (in two dimensions $1 < \rho_0\lambda^2 < 350$). In this regime there is some interpenetration of initially correlated reactant pairs. At time t_c a slow burst begins that builds up over a much longer time than in the previous case, as seen in our simulations.

We now discuss the situation when $\rho_0\lambda^d$ is large ($\rho_0 \gg 6$ in one dimension, $\rho_0\lambda^2 \gg 350$ in two dimensions), so that $t_s < t_c$ (Figure 2). In this regime the A + B reaction behaves quite differently from the A + A reaction for times $t \geq t_s$. At time t_s segregation begins, and the segregated aggregates grow in size as they would in the case of random initial conditions. However, this growth stops at a time $t \sim t_c = \lambda^2/8D$, when the aggregates are of linear size $\sim \lambda$. At this time the aggregates actually begin to shrink. The shrinkage continues until a single particle per aggregate

remains; that is, A and B particles are arranged in an essentially latticelike way with "lattice constant" λ . This occurs at a time that we call t_{es} . Within a time of order $\lambda^2/2D$ beyond this, at a time that we call t_{sb} , a slow burst begins which eventually ends in either an A + A-like uncorrelated behavior or with finite lattice size behavior. This description is again quantitatively borne out by our simulations.

As the difference between t_s and t_c decreases (that is, as $\rho_0\lambda^d$ becomes smaller), the behavior described in the progression of Figure 2 smoothly merges into that of Figure 4; at first with no segregation regime but still with a slow burst. In turn, with a further decrease in $\rho_0\lambda^d$ the slow burst behavior smoothly merges into the fast burst. These transitions are also observed in our simulations.

Let us finally summarize our major results. For completeness we include a summary of our results for the random initial condition case.³¹

For random initial conditions we found three main novel features:

1. At early times the A + B \rightarrow 0 system does *not* segregate. Instead it behaves exactly as does the A + A \rightarrow 0 system, with both classical t^{-1} and nonclassical $t^{-d/2}$ (for $d \leq 2$) behavior.
2. This behavior stops at a time t_s , when the segregation process begins. We have found scaling laws for t_s and for the density ρ_s at time t_s . Our simulations yield the unknown dimension-specific parameters for $d = 1$ and $d = 2$.
3. Eventually, finite system size effects set in when the segregated aggregates are within an order of magnitude of the size of the system (linear dimension) at a time t_f whose scaling behavior we have confirmed. Again, we have determined dimension-specific parameters for $d = 1$ and $d = 2$ from our simulations. These results provide information on the segregation process in infinite lattices.

Our simulations are in excellent agreement with our theoretical predictions.

For correlated initial conditions we have clarified the variety and complexity of different time progressions as a function of the initial conditions. The most important characterizing parameter is the product $\rho_0\lambda^d$ of the initial density and the correlation volume. If this product is small we find the following principal features:

1. The A + B \rightarrow 0 reaction proceeds exactly as does the A + A \rightarrow 0 reaction for the same values of ρ_0 and λ . In particular, there is no segregation in the A + B system in this case. Neither one of these two reactions has been studied before in this regime to the best of our knowledge.
2. At early times the behavior is that of the uncorrelated A + A problem, again including both classical and nonclassical regimes. At time $t_c = \lambda^2/8D$, an increase (burst) in the reaction rate is observed which arises from the annihilation of correlated pairs.
3. Once the burst is over the behavior settles back to the uncorrelated nonclassical A + A form and/or behavior produced by finite system size effects. When $\rho_0\lambda^d$ is large, segregation does occur in the A + B \rightarrow 0 reaction. The progression of events is as follows:
 1. At early times the A + B \rightarrow 0 reaction again (as always) behaves the same as the A + A \rightarrow 0 reaction (classical, $t^{-d/2}$).
 2. The A + B system departs from this behavior at the same time t_s determined in the random initial condition problem, and segregation begins ($t^{-d/4}$).
 3. The segregation process is halted at time $t_c = \lambda^2/8D$, when the aggregates, which at this point are of linear size $\sim \lambda$, actually begin to shrink ($t^{-(d+2)/4}$) until only one particle per aggregate remains at time t_{es} .
 4. At a time t_{sb} which is of order $\lambda^2/2D$ beyond t_{es} there is a (slow) burst when these remaining particles meet. These are not

the originally correlated particles so one might call this a "burst echo" or "delayed burst".

5. Once the burst has exhausted itself, the nonclassical $A + A$ behavior resumes and/or finite size effects take over.

Acknowledgment. We gratefully acknowledge support from the U.S. Department of Energy Grant No. DE-FG03-86ER13606 (K.L.), from the National Science Foundation Grant No. DMR-91-11622 (R.K.), and from NATO grant No. CRG 920029 (P.A.).

References and Notes

- (1) Kopelman, R. *Science* **1988**, *241*, 1620.
- (2) For a review see, for example: Kuzovkov, V.; Kotomin, E. *Rep. Prog. Phys.* **1988**, *51*, 1479 and references therein.
- (3) Ovchinnikov, A. A.; Zeldovich, Y. G. *Chem. Phys.* **1978**, *28*, 215.
- (4) Toussaint, D.; Wilczek, F. *J. Chem. Phys.* **1983**, *78*, 2642.
- (5) Kang, K.; Redner, S. *Phys. Rev. Lett.* **1984**, *52*, 955.
- (6) Lindenberg, K.; West, B. J.; Kopelman, R. In *Noise and Chaos in Nonlinear Dynamical Systems*; Capelin, S., Moss, F., Eds.; Cambridge University Press: Cambridge, U.K., 1989, and references therein.
- (7) Clément, E.; Sander, L. M.; Kopelman, R. *Phys. Rev. A* **1989**, *39*, 6455; *ibid.*, 6466.
- (8) Clément, E.; Sander, L. M.; Kopelman, R. *Phys. Rev. A* **1989**, *39*, 6472.
- (9) Sheu, W.-S.; Lindenberg, K.; Kopelman, R. *Phys. Rev. A* **1990**, *42*, 2279.
- (10) Bramson, M.; Lebowitz, J. L. *J. Stat. Phys.* **1991**, *62*, 297.
- (11) Zumofen, G.; Klafter, J.; Blumen, A. *Phys. Rev. A* **1992**, *45*, 8977.
- (12) Anacker, L. W.; Kopelman, R. *Phys. Rev. Lett.* **1987**, *58*, 289.
- (13) Jiang, Z.; Ebner, C. *Phys. Rev. A* **1990**, *41*, 5333.
- (14) Argyrakis, P.; Kopelman, R. In *Dynamics in Small Confining Systems*; Drake, J. M., Klafter, J., Kopelman, R., Eds.; Materials Research Society: Pittsburgh, 1990; p 195.
- (15) Argyrakis, P.; Kopelman, R. *Phys. Rev. A* **1990**, *41*, 2114, 2121.
- (16) Leyvraz, F.; Redner, S. *Phys. Rev. Lett.* **1991**, *66*, 2168.
- (17) Kanno, S. *Prog. Theor. Phys.* **1988**, *79*, 721, 1330.
- (18) Lin, J.-C.; Doering, C. R.; Ben-Avraham, D. *Chem. Phys.* **1990**, *146*, 355.
- (19) Doering, C. R.; Ben-Avraham, D. *Phys. Rev. A* **1988**, *38*, 3035.
- (20) Lindenberg, K.; Sheu, W.-S.; Kopelman, R. *J. Stat. Phys.* **1991**, *65*, 1269.
- (21) Klymko, P.; Kopelman, R. *J. Phys. Chem.* **1982**, *86*, 3686; **1983**, *87*, 4565.
- (22) Torney, D. C.; McConnel, H. M. *J. Phys. Chem.* **1983**, *87*, 1441.
- (23) Kopelman, R. *J. Stat. Phys.* **1986**, *42*, 185.
- (24) Anacker, L. W.; Kopelman, R. *J. Chem. Phys.* **1984**, *81*, 6402.
- (25) Anacker, L. W.; Parson, R. P.; Kopelman, R. *J. Phys. Chem.* **1985**, *89*, 4758.
- (26) Evesque, P.; Duran, J. *J. Chem. Phys.* **1984**, *80*, 3016. Klymko, P. W.; Kopelman, R. *J. Phys. Chem.* **1983**, *87*, 4565.
- (27) Kopelman, R.; Parus, S. J.; Prasad, J. *Chem. Phys.* **1988**, *128*, 209.
- (28) Chandrasekhar, S. *Rev. Mod. Phys.* **1943**, *15*, 1.
- (29) Argyrakis, P.; Kopelman, R. *J. Phys. Chem.* **1989**, *93*, 225.
- (30) Lindenberg, K.; West, B. J.; Kopelman, R. *Phys. Rev. A* **1990**, *42*, 890.
- (31) Argyrakis, P.; Kopelman, R.; Lindenberg, K. *Chem. Phys.* **1993**, *177*, 693.
- (32) Lindenberg, K.; West, B. J.; Kopelman, R. *Phys. Rev. Lett.* **1988**, *60*, 1777.
- (33) Lindenberg, K.; Kopelman, R.; Argyrakis, P. In *Fluctuations and Order: The New Synthesis*; Millonas, M. M., Ed.; Springer-Verlag: New York, in press.
- (34) Argyrakis, P.; Kopelman, R. *Phys. Rev. A* **1992**, *45*, 5814.
- (35) Argyrakis, P. *Comput. Sci.* **1992**, *6*, 525.
- (36) Schoonover, R.; Ben-Avraham, D.; Havlin, S.; Kopelman, R.; Weiss, G. H. *Physica A* **1991**, *171*, 232 and references therein.
- (37) Torney, D. C.; McConnel, H. M. *Proc. R. Soc. London, Ser. A* **1983**, *387*, 147.
- (38) Kopelman, R.; Argyrakis, P. *J. Chem. Phys.* **1980**, *72*, 3053.